

---

---

## RECOGNITION OF GEOMAGNETIC STORMS FROM TIME SERIES OF MATRIX OBSERVATIONS WITH THE MUON HODOSCOPE URAGAN USING NEURAL NETWORKS OF DEEP LEARNING

**V.G. Getmanov**

Geophysical Center RAS,  
Moscow, Russia, v.getmanov@gcras.ru  
Schmidt Institute of Physics of the Earth RAS,  
Moscow, Russia

**A.D. Gvishiani**

Geophysical Center RAS,  
Moscow, Russia, a.gvishiani@gcras.ru  
Schmidt Institute of Physics of the Earth RAS,  
Moscow, Russia

**A.A. Soloviev**

Geophysical Center RAS,  
Moscow, Russia, a.soloviev@gcras.ru  
Schmidt Institute of Physics of the Earth RAS,  
Moscow, Russia

**K.S. Zajtsev**

National Research Nuclear University MEPhI,  
Moscow, Russia,  
kszajtsev@mephi.ru

**M.E. Dunaev**

National Research Nuclear University MEPhI,  
Moscow, Russia,  
dunaev@mail.ru

**E.V. Ehlakov**

National Research Nuclear University MEPhI,  
Moscow, Russia,  
fruha1980@gmail.com

---

**Abstract.** We solve the problem of recognizing geomagnetic storms from time series of matrix observations with the URAGAN muon hodoscope, using deep learning neural networks. A variant of the neural network software module is selected and its parameters are determined. Geomagnetic storms are recognized using binary classification procedures; a decision-making rule is formed. We estimate probabilities of correct and false recognitions. The recognition of geomagnetic storms is experimentally studied; for the assigned  $Dst$  threshold  $Y_{D0} = -45$  nT we obtain acceptable probabilities of cor-

rect and false recognitions, which amount to  $\beta = 0.8212$  and  $\alpha = 0.0047$ . We confirm the effectiveness and prospects of the proposed neural network approach.

**Keywords:** geomagnetic storms, recognition, neural networks, probabilities of correct and false recognitions, matrix observations, muon hodoscope.

---

### INTRODUCTION

The paper discusses the recognition of geomagnetic storms (GMS) through digital processing of matrix data sets from the muon hodoscope (MH) URAGAN, using deep learning neural networks (DLNN). We interpret the recognition as a problem consisting in making decisions about the presence or absence of GMS for a given moment in time from MH observations.

The GMS recognition based on neural digital processing of matrix MH observations is an urgent scientific problem in solar-terrestrial physics.

Geomagnetic disturbances are generated by the impact of plasma formations from solar coronal mass ejections on Earth's magnetosphere. GMS are geomagnetic disturbances whose amplitudes are, on average, higher than a given one.

As is known, activity of the geomagnetic field is characterized by geomagnetic indices. One of the most common is the hourly  $Dst$  index, introduced and described in [Suigiura, 1964]. It is determined from the geomagnetic field vector components from four longitudinally-spaced equatorial magnetic observatories and is calculated by averaging with 1-hour discreteness.  $Dst$  indices are measured in nanoteslas: for the undisturbed

magnetosphere  $Dst = +20 \div -40$  nT; for GMS,  $-50 \div -150$  nT; in exceptional cases, they go beyond the given range. The time series of the  $Dst$  indices was taken from the WDCG (World Data Center of Geomagnetism, Kyoto) website [<https://wdc.kugi.kyoto-u.ac.jp>].

Neural networks are often used to solve problems of solar-terrestrial physics [Barkhatov, 2010; Bernhardt, 2022]. A number of publications in the subject area of interest, which are related to neural networks, are distinguished by information sources, neural network structures, versions of problems, and possibilities for obtaining solutions without constructing any physical models, which can be successfully applied to complex geophysical systems.

The works [Palloch et al., 2006; Lundstredt, 1997] are devoted to the neural network analysis of GMS based on solar wind data and multilayer perceptrons. Gruet et al. [2018] presents a method combining a recurrent NN with short-term memory and a Gaussian process model for evaluating characteristics of  $Dst$  indices. Stepanova and Perez [2000] use a multilayer perceptron to examine  $Dst$  variations several hours ahead. In [Efitorov et al., 2018; Dolenko et al., 2005; Myagkova et al., 2021], the possibilities are explored of employing time series of geomagnetic  $Dst$  indices and

their relationships with parameters, as well as methods of NN machine learning with classical perceptrons and recurrent networks.

In [Belov et al., 2022; Getmanov et al., 2022a], an approach is described which consists in using scalar time series of MH observations and convolutional NN for analyzing GMS. Implementation of the proposed approach to GMS recognition using time series of matrix MH observations and deep learning NN aims to demonstrate its efficiency and possible future prospects.

## 1. OBSERVATIONS WITH THE URAGAN MUON HODOSCOPE AND GM RECOGNITION PROBLEM SOLVING BASED ON NN TECHNOLOGIES

In this paper, the GMS recognition is based on observations with the muon hodoscope URAGAN [Yashin et al., 2015], designed at MEFhI. Muons are elementary particles formed due to nuclear reactions between relativistic cosmic protons and individual atomic nuclei, which are part of Earth's upper atmosphere [Murzin, 2007; Astapov et al., 2014]. The muon hodoscope URAGAN is a computer-aided measuring device that determines the muon flux (MF) by counting the number of muons incident on the MH aperture for a given system of solid angles and a specified time discrete. The time-varying estimated MFs obtained from MH observations provide information about extreme heliospheric events and possible upcoming GMS.

The results of counting the number of muons with MH are formed into a time series of primary initial matrix MH observations  $X(i, j, T_{rg}, T_k)$ , consisting of Poisson numbers  $i=1, \dots, N_1, j=1, \dots, N_2, N_1=90, N_2=76; T$  is the specified time discrete;  $k$  is the time index; generally,  $T=1/60$  hr (1 min);  $T_{rg}=58.5$  s is the muon detection (counting) interval length.

The azimuth and zenith indices  $i, j$  define the system of solid angles  $\varphi_i=\Delta\varphi(i, 1), \vartheta_j=\delta\vartheta(j-1), \Delta\varphi=1^\circ, \delta\vartheta=4^\circ, i=1, \dots, N_1, j=1, \dots, N_2$  in which MF is estimated. The collected muons corresponding to  $\varphi_i, \vartheta_j$  are placed discretely in  $(i, j)$  cells for MH matrices.

The primary 1-minute normalized matrix MH observations  $X(i, j, T_k)$  are formed from initial MH observations and determine the number of detected particles for the indices  $i, j$  reduced to 1 s,

$$X(i, j, T_k) = X(i, j, T_{rg}, T_k) / T_{rg}, k = 1, 2, \dots \quad (1)$$

The time series of secondary hourly normalized matrix MH observations is derived from minute observations (1) by averaging them over a 60-min time interval  $T_0=60T$ .

$$X(i, j, T_0n) = \sum_{k=k_1(n)}^{k_2(n)} X(i, j, T_k) / 60, \quad (2)$$

$$k_1(n) = 1 + 60(n-1), k_2(n) = 60n, n = 1, 2, \dots$$

We deal with modulation and noise disturbances in time series of hourly normalized matrix MH observa-

tions  $X(i, j, T_0n)$  (2) taken from the Data Base of Muon Hodoscope MEFhI [https://www.nevod.mephi.ru/]. The time series was formed from matrix MH observations with an initial index  $n=1$  corresponding to January 01, 2013, 00:00 UT.

Figure 1 presents a 2D image of the hourly normalized MH observation matrix  $X(i, j, T_0n_0), i=1, \dots, N_1, j=1, \dots, N_2$ , obtained from the given time series for  $n_0=50300$ . The 2D function  $X(i, j, T_0n)$  is seen to contain significant modulations and noise. Matrix elements for zenith angles with  $j \approx 25 \div 30$  take maximum values; for zenith angles with  $j \approx 1 \div 2, 75 \div 76$ , minimum values differing tenfold. Azimuth modulations for  $X(i, j, T_0n_0)$  are much less than zenith modulations.

Figure 2 plots a 1D function of average hourly MH observations  $S(T_0n)$ , which was calculated on a 1-month period with  $n_1=50100, n_2=50800$  from

$$S(T_0n) = \frac{1}{N_1 N_2} \sum_{i=1}^{N_1} \sum_{j=1}^{N_2} X(i, j, T_0n), n_1 \leq n \leq n_2. \quad (3)$$

There are  $\sim 30$  periods of noisy diurnal oscillations of the  $S(T_0n)$  function here. In the GMS catalog [http://www.izmiran.ru/ionosphere/weather/storm.2023], we can find information that a rather complex geomagnetic situation took place in the 1-month period — three

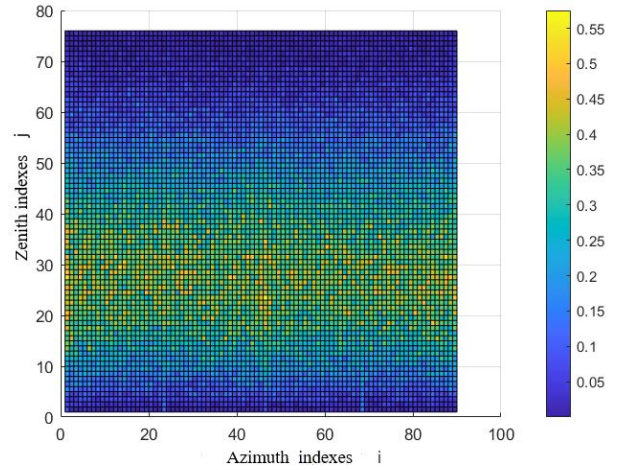


Figure 1. A 2D image of hourly normalized MH observation matrix  $X(i, j, T_0n_0)$

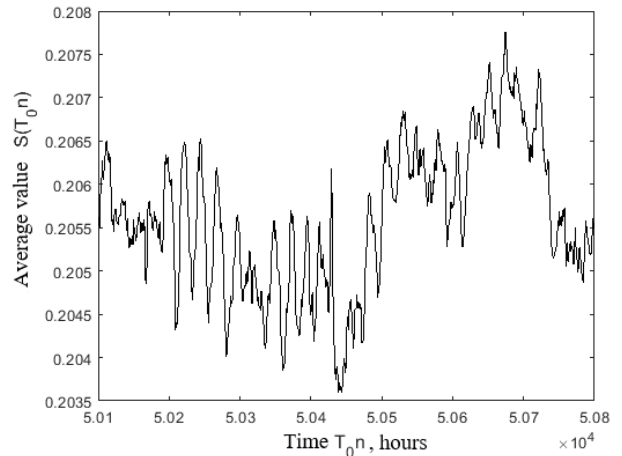


Figure 2. One-dimensional function of average hourly MH observations  $S(T_0n)$

*Dst* storms occurred. Figure 2 indicates that MH observations respond in a certain way to GMS. Note that minimum and maximum  $S(T_0n)$  differed by only  $\sim 1.9\%$ . We can deduce that the recognition of modulations from GMS in modulated and noisy time series of matrix MH observations by the use of traditional time-frequency technologies is largely problematic.

Two solutions of the problem of GMS recognition are allowed which are based on time series of matrix MH observations and NN technologies. The former involves the formation of time series of  $S(T_0n)$  from (3) from matrix MH observations. This solution [Belov et al., 2022; Getmanov et al., 2022a] can reduce computer requirements for NN implementation, but by decreasing the efficiency of GMS recognition. The second implies the direct use of time series of matrix MH observations, which requires high-performance computers capable of increasing the efficiency of GMS recognition for NN. In this case, the second solution is taken as a basis.

Note that the publications [Chinkin et al., 2019, Getmanov et al., 2022a] have addressed the problems of detecting the so-called local anisotropies for MF, which we have used as the methodological framework for this paper.

## 2. ALGORITHM OF CALCULATION OPERATIONS IN GMS RECOGNITION PROBLEM SOLVING; ResNet34

The algorithm for solving the GMS recognition problem is based on the assumption that there is a complex noisy relationship between MH observations and *Dst* indices. In the paper, we construct a model of the relationship between *Dst* indices and MH observations, using the deep learning NN.

We employ the time series of matrix MH observations  $X(i, j, T_0n)=X_M(n)$  and the time series of scalar *Dst* indices  $Y_D(n)$ , which are formed in the international reference time scale UTC. Sampling is carried out for  $T_0n$ .

MH observations  $X_M(n)$  and *Dst* indices  $Y_D(n)$  are determined in a nine-year period. At the training stage with  $1 \leq n \leq n_{f0}$ ,  $n_{f0}=62128$ , MH observations and *Dst* indices are used; the result of this stage is the NN model. At the testing stage, MH observations with  $n_{f0}+1 \leq n \leq n_{f1}$ ,  $n_{f1}=70128$  are employed; at this stage, the learning stage of the constructed NN model is controlled. At the validation stage, MH observations are applied to  $n_{f1}+1 \leq n \leq n_f$ ,  $n_f=78888$ ; model estimates of *Dst* indices are calculated  $Y_D^\circ(n)$  by the NN

model and only from the dataset  $X_M(n)$ , *Dst* indices are used only to assess the probabilities of recognizing GMS.

The algorithm of the GMS recognition problem solving consists of four stages.

At stage 1, preliminary digital processing is performed for the initial time series of matrix MH observations  $X_M(n)$  and the time series of *Dst* indices  $Y_D(n)$ ; they are filtered to eliminate low-frequency and high-frequency noise and are scaled up to ensure the commensurability of variables necessary for effective NN training. The preprocessing results are denoted as  $X_{M1}$ ,  $X_{M2}$ ,  $Y_{D1}$ .

At stage 2, NN training and testing are implemented. We use the matrix time series  $X_{M1}$  and the training scalar time series  $Y_{D1}$ ,  $1 \leq n \leq n_{f1}$ . The NN model is formed and its quality is assessed.

At stage 3, validation stage, *Dst* indices are estimated  $Y_D^\circ$ . Here, we employ the variables  $X_{M2}$  on the interval  $n_{f1}+1 \leq n \leq n_f$  and the NN model constructed at the previous stage.

At stage 4, the decision-making procedure for GMS recognition is implemented by comparing the calculated model estimates of *Dst* indices  $Y_D^\circ(n)$  with the assigned threshold  $Y_{D0}$ .

Figure 3 shows an enlarged diagram of the neural network algorithm for calculation operations with the above variables, which explains the GMS recognition problem solving.

The results of the formulated GMS recognition problem solving, which are related to the digital processing of a large amount of data, have been obtained using cloud technologies. The MEPhi Supercomputer Center was employed to perform resource-intensive computing [https://it.mephi.ru/hpc/performance], required for DLNN.

A DLNN version based on the Python programming language and the PyTorch module library was developed. We examined the following network software modules: EfficientNet [https://arxiv.org/abs/1905.11946], VGG [https://arxiv.org/abs/1409.1556v6], DenseNet [https://arxiv.org/abs/1608.06993v5], Inception-v3, and ResNet [https://arxiv.org/abs/1512.00567v3] from this library. The network software module ResNet and its modification ResNet34 were taken for implementation. This module has a high accuracy and a small number of trained parameters as compared to other modules mentioned above. ResNet34 was chosen due to the fact that in the studies of training of these neural networks this module was in second place, working without augmentation

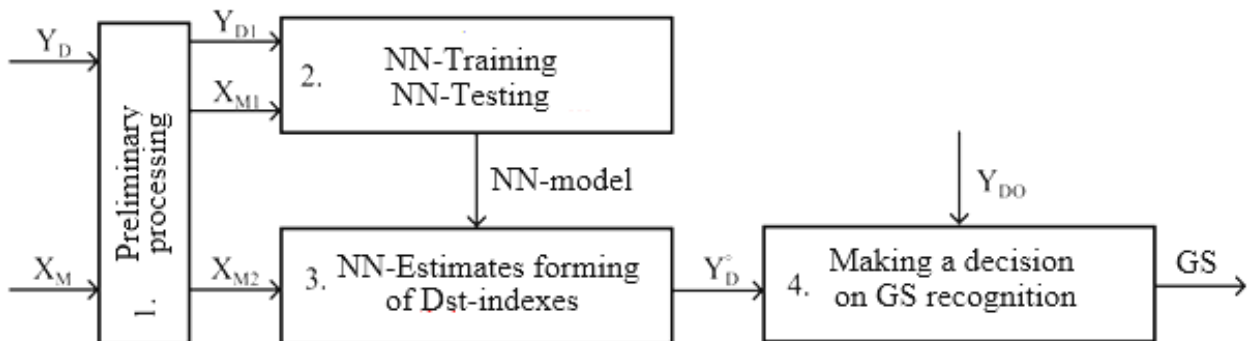


Figure 3. Diagram of the algorithm of calculation operations for solving the GMS recognition problem

[<https://arxiv.org/pdf/2107.07699.pdf>]. ResNet34 is described in general at [<https://arxiv.org/abs/1512.03385>].

Dimension of the input matrix package  $\Delta n$  was specified by analyzing the results of preliminary computational experiments with NN ResNet34 and available MH observations. At the NN output, model estimates of  $Dst$  indices were developed  $Y_D^\circ$  which were then applied to the GMS recognition problem.

### 3. TRAINING, TESTING, VALIDATION, AND QUALITY METRICS

#### Characteristics

The selected NN was trained to calculate the optimal weight coefficients of the NN model. The gradient descent search algorithm Adam was used; the algorithm parameters  $\alpha_E=0.001$ ,  $\beta_1=0.9$ ,  $\beta_2=0.999$  were taken; the default value was  $\varepsilon=10^{-8}$  from [<https://arxiv.org/pdf/1412.6980.pdf>]. Parameter  $\alpha_E$  is the learning rate,  $\beta_1$  is the exponential decay for estimating the first moment,  $\beta_2$  is the exponential decay for estimating the second moment,  $\varepsilon$  is the parameter added to the denominator to improve numerical stability, used to control the gradient descent procedure [<https://pytorch.org/docs/stable/generated/torch.optim.Adam.html>; Ba, Kingma, 2015].

The number of free parameters of the implemented learning model was 21.5 millions — this number was calculated by code, namely by summing up the number of trained parameters of each block of the model. The volume of the training dataset was  $N_1 \times N_2 \times$  the total number of hours in the dataset — obviously, the volume of this dataset for training significantly exceeded the given number of parameters.

Testing was carried out to determine the quality of the NN model constructed at the training stage. This stage employed a testing dataset other than the training and validation datasets.

The constructed NN model was validated by calculating model estimates of  $Dst$  indices  $Y_D^\circ$ . A time series was formed from them and binary classification procedures were applied to its elements to recognize GMS [<https://www.learnatasci.com/glossary/binary-classification/>]. We compared  $Y_D^\circ(n)$  with  $Y_{D0}$ .

According to conditions of the problem, at the validation stage the initial  $Dst$  indices were used only for numerically estimating the probabilities of recognizing GMS. In this regard, from the inequalities

$$Y_D(n) \leq Y_{D0}, \quad n_{f1} + \Delta n + 1 \leq n \leq n_f \quad (4)$$

we calculated the number of indices with GMS events  $N_{1,GMS}$  and the number of indices without GMS events  $N_{0,GMS}$ .

We calculated the number of correct GMS recognitions  $N_{R,GMS}$  and the number of false ones  $N_{F,GMS}$ , taking into account that in this case it was known in advance whether there was or was not a GMS event for each  $n$ .

We introduced the probabilities of  $\beta$  correct and  $\alpha$

false GMS recognitions in the form of the following obvious formulas

$$\beta = N_{R,GMS} / N_{1,GMS}, \quad \alpha = N_{F,GMS} / N_{0,GMS}.$$

*Error function.* The NN model's parameters were optimized using error function values. In general, for regression problems we took a function designated as *RMSE* [Chen et al., 2022] and representing the root-mean-square error, the difference between model estimates  $Y_D^\circ(n)$  and actual variables, for the error function  $Y_D(n)$ .

$$RMSE = \left(1 / (n_f - n_{f1} - \Delta n)\right) \times \sum_{n=n_{f1}-\Delta n}^{n_f} \left(Y_D^\circ(n) - Y_D(n)\right)^2.$$

Computational experiments have shown that the first-order Adam gradient optimization method, we adopt here, for this loss function worked satisfactorily in practice and set apart from other stochastic optimization methods. This method is easy to implement, computationally effective, and well suited for problems with large amounts of data with convergence comparable to the best known results in convex optimization procedures.

The training was stopped through visual analysis of error function values when the *RMSE* plot moved to a plateau; at the same time, testing implemented control over the absence of retraining.

*Quality metrics.* We have determined the recognition quality metric by analogy with the Recall metric from [[https://en.wikipedia.org/wiki/Binary\\_classification](https://en.wikipedia.org/wiki/Binary_classification)].

Taking into account the formulation of the problem to be solved, the quality metric was taken as

$$G0(\alpha, \beta) = \beta + 1 - \alpha, \quad (5)$$

whose content is completely transparent from a physical point of view. It follows from the last expression that with increasing probability  $\beta$  and decreasing probability  $\alpha$ , the quality metric  $G0(\alpha, \beta)$  increases.

The  $G0$  binary classification quality metric is usually applied to the so-called balanced data distributed evenly. In case of a possible data imbalance, this metric greatly distorts the actual quality of the classification. It is worthwhile examining the solution of the proposed problem for comparison on the basis of the  $G1$  metric, which is weakly sensitive to data imbalance. According to [[https://helenkapatsa.ru/otsienka\\_f1](https://helenkapatsa.ru/otsienka_f1)],  $G1(\alpha, \beta)$  is written as

$$G1(\alpha, \beta) = 2A(\alpha, \beta)R(\alpha, \beta) / (A(\alpha, \beta) + R(\alpha, \beta)), \quad (6)$$

where

$$A(\alpha, \beta) = TP / (TP + FP),$$

$$R(\alpha, \beta) = TP / (TP + FN),$$

$$TP = \beta, \quad NP = 1 - \alpha, \quad FP = 1 - \beta, \quad FN = \alpha.$$

#### 4. STOPPING THE TRAINING BASED ON THE RMSE METRIC; ESTIMATED PROBABILITIES OF CORRECT AND FALSE GMS RECOGNITION; CALCULATING G0, G1 QUALITY METRICS

The training stage was stopped based on the error function calculations obtained from NN training. The error functions for the training and validation samples were designated as  $RMSE1(N_E)$  and  $RMSE2(N_E)$  respectively, where  $N_E$  is the number of epochs. Visual analysis of the calculated estimates was implemented.

Figure 4 shows  $RMSE1(N_E)$  calculated for the training stage dataset and  $RMSE2(N_E)$  for the validation stage dataset.

The visual analysis of the plots allowed us to

1) decide on the optimum number of epochs for the training stage  $N_E^\circ = 20$ , for the validation stage  $N_E^\circ = 30$ ;

2) conclude about the absence of the NN model re-training.

Probabilities of correct and false GMS recognition were assessed. The threshold  $Y_{D0}$  was established and the time point with  $n$  for which GMS occurred was studied when comparing  $Y_D(n) \leq Y_{D0}$  from (4). The number of  $N_{1,GMS}$  states with GMS was determined by counting the fulfillment of this inequality in the control period for  $n_{f1} + \Delta n + 1 \leq n \leq n_f$ , where  $\Delta n$  is the dimension of the input matrix package.

We carried out the sum operation

$$N_{1,GMS} = \sum_{n=n_{f1}+\Delta n+1}^{n_f} H(Y_{D0} - Y_D(n)), \quad (7)$$

where  $H(x)$  is the Heaviside function  $H(x)=1, x \geq 0, H(x)=0, x < 0$ . The number of  $N_{0,GMS}$  states without GMS on the interval  $n_{f1} + \Delta n + 1 \leq n \leq n_f$  was found from  $N_{0,GMS} = n_f - n_{f1} - \Delta n - 1 - N_{1,GMS}$ .

We determined  $N_{R,GMS}$  — the number of correct GMS recognitions from estimated  $Dst$  indices  $Y_D^\circ(n)$  and  $\beta$  — estimated probability of correct GMS recognition, by summing and calculating the relation

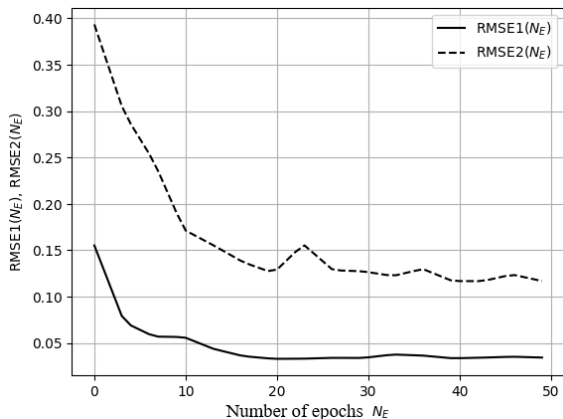


Figure 4. Estimated  $RMSE1(N_E)$  and  $RMSE2(N_E)$  for training and validation stages

$$N_{R,GMS} = \sum_{n=n_{f1}+\Delta n+1}^{n_f} H(Y_{D0} - Y_D(n))H(Y_{D0} - Y_D^\circ(n)), \quad (8)$$

$$\beta = \frac{N_{R,GMS}}{N_{1,GMS}}.$$

$N_{F,GMS}$  — the number of false GMS recognitions and  $\alpha$  — estimated probability of false GMS recognition were found as in (8)

$$N_{F,GMS} = \sum_{n=n_{f1}+\Delta n+1}^{n_f} H(Y_D(n) - Y_{D0})H(Y_{D0} - Y_D^\circ(n)), \quad (9)$$

$$\alpha = \frac{N_{F,GMS}}{N_{0,GMS}}.$$

The quality metrics  $G0, G1$  (5), (6) were calculated in the control period with  $n_{f1} + \Delta n + 1 \leq n \leq n_f$  from the dataset  $X_M(n)$ . For this purpose, we estimated the model  $Dst$  indices  $Y_{D0}^\circ(n)$  and compared them with  $Y_{D0}$ .

According to Section 3, we assigned the dimension of input matrix package  $\Delta n=60$ , which remains the same for calculations throughout the paper. We calculated discrete values of the recognition threshold  $Y_{D0}(l) = \bar{Y}_{D1} + \Delta Y_{D0}(L-1), \bar{Y}_{D1} = -70$  nT,  $\Delta Y_{D0} = 5$  nT,  $l=1, 2, \dots, 9$ . We estimated  $\beta(Y_{D0}(l))$  and  $\alpha(Y_{D0}(l))$  probabilities of correct and false GMS recognition, using formulas (7)–(9) depending on  $Y_{D0}(l)$  parameters.

Figure 5,  $a, b$  presents the results of calculations of estimated probabilities  $\beta(Y_{D0})$  and  $\alpha(Y_{D0})$  depending on  $Y_{D0}$ . Obviously, the estimated probabilities increase with increasing threshold. The calculations have led us to conclude that for  $-70 \leq Y_{D0} \leq -50$  nT the average probability of false GMS recognition  $\alpha \approx 0.001$ , whereas the probability of correct recognition  $0.575 \leq \beta \leq 0.75$ ; for  $Y_{D0} = -37.5$  nT,  $\alpha \approx 0.02, \beta \approx 0.875$ ; for  $Y_{D0} = -34.0$  nT,  $\alpha \approx 0.045, \beta \approx 0.91$ .

Using estimated  $\beta(Y_{D0}), \alpha(Y_{D0})$ , we evaluated metrics (5), (6)  $G0$ , and  $G1$  depending on  $Y_{D0}$ . We plotted them and compared the metrics.

Studying the estimated metrics in Figure 6,  $a, b$  has led us to the following conclusions: 1) the metrics  $G0$  and  $G1$  turned out to be close differing by about a constant when comparing their dependence on the recognition threshold  $Y_{D0}$ ; the possible assumption that the initial MH observations were unbalanced proved to be insufficiently accurate and contradicted the calculations of the metrics; 2) analyzing positions of maxima on the plots of the metrics determined the optimum recognition threshold (in terms of  $G0$  and  $G1$ ), which was  $Y_{D0}^\circ \approx -35$  nT.

#### 5. ESTIMATING MODEL Dst INDICES AND GMS RECOGNITION RESULTS

We have chosen a six month period 2021.07.01–2022.01.01, which is within the boundaries of the control period. Figure 7 displays real  $Y_D = Y_D(T_0/n)$  and model

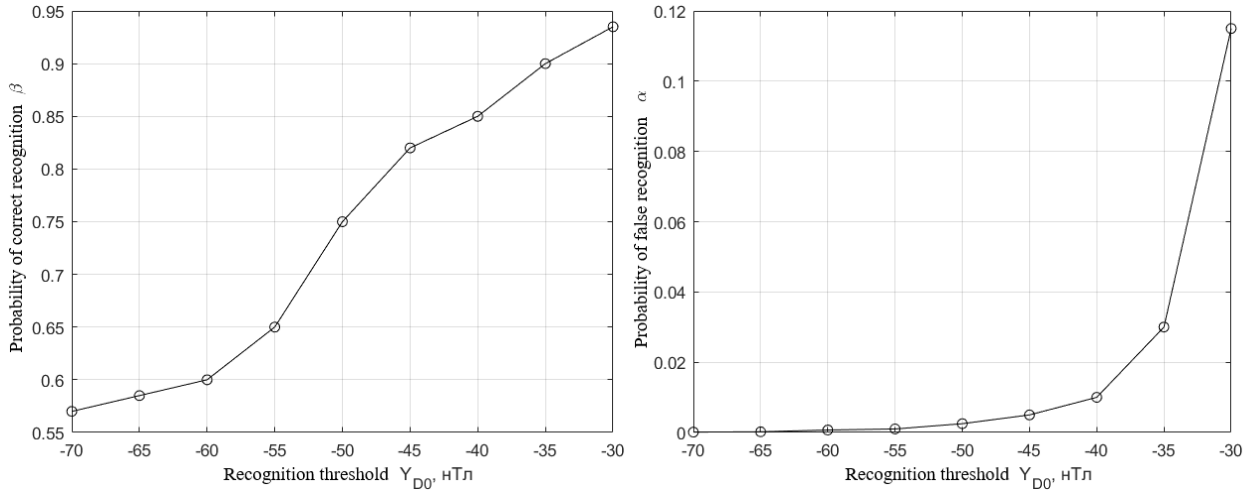


Figure 5. Results of estimated correct  $\beta(Y_{D_0})$  (a) and false  $\alpha(Y_{D_0})$  (b) GMS recognitions

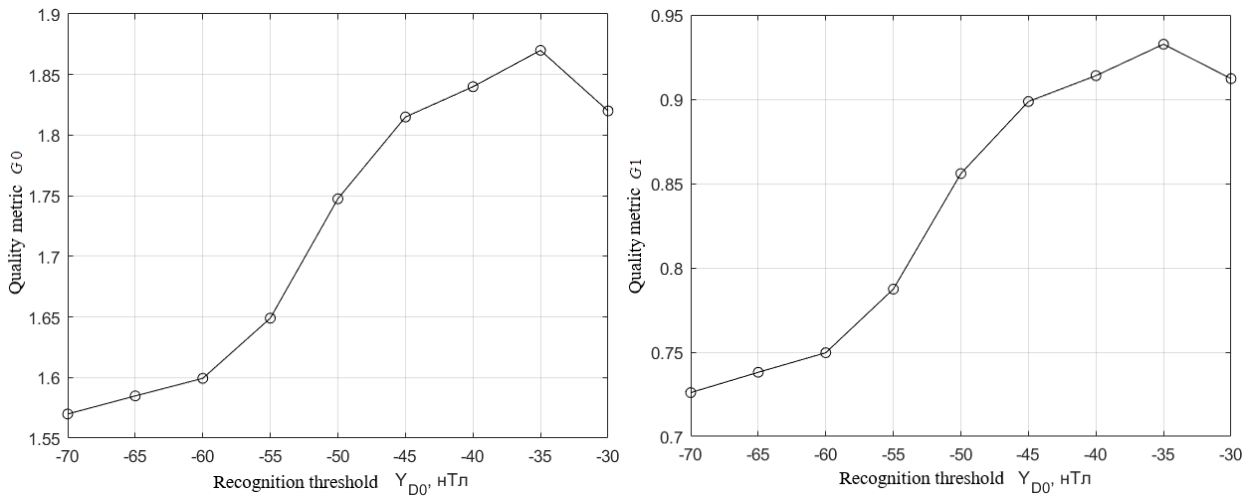


Figure 6. Metrics  $G_0$  (a) and  $G_1$  (b) as a function of the recognition threshold  $Y_{D_0}$

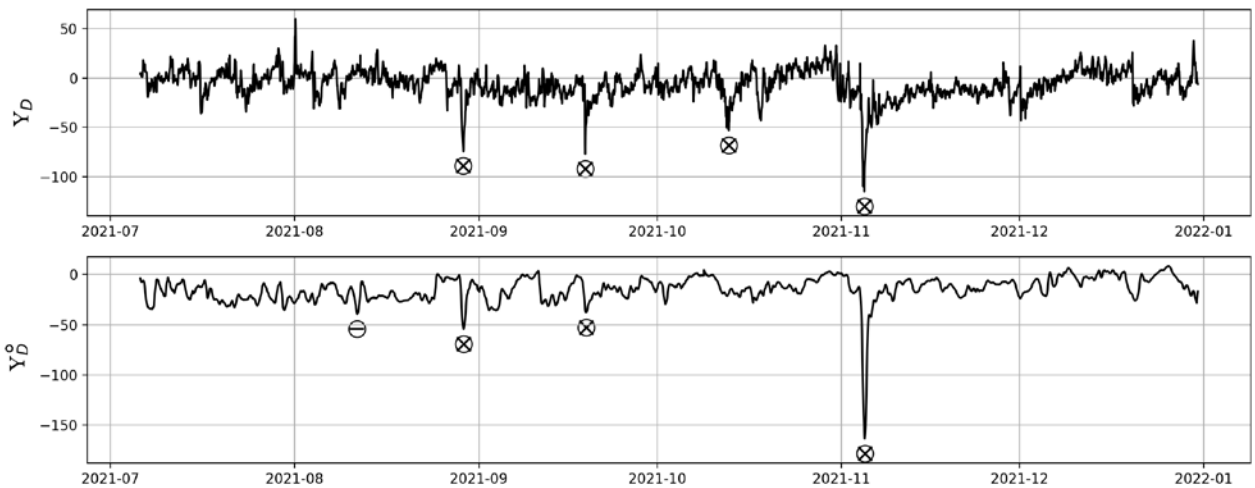


Figure 7. Real  $Y_D(T_0 n)$  and model  $Y_{D_0}^\circ(T_0 n)$  Dst indices

$Y_{D_0}^\circ = Y_{D_0}^\circ(T_0 n)$  Dst indices. For  $Y_{D_0} = -45$  nT, four GMS events occurred during the period of interest (marked with crosses in circles).

The plot  $Y_{D_0}^\circ(T_0 n)$  in view of  $Y_{D_0}$  shows that there are

three correct GMS recognitions, one false (marked with minus in a circle) and one omission of correct GMS recognition. Using (7)–(9), we estimated the probabilities of correct and false GMS recognitions.

The results of calculations using the developed algo-

rithm for a six-month time period, taking into account the assigned threshold  $Y_{D0} = -45$  nT and the results of calculations with Figure 6, *a*, *b*, enabled us to make certain of obtaining acceptable estimates of the probabilities of correct and false recognitions:  $\beta \approx 0.8212$  and  $\alpha \approx 0.0047$ .

Analysis of the algorithm for calculating the probabilities of correct and false GMS recognitions and experimental study of the results of GMS recognition have led us to conclude that the proposed neural network approach proved to be largely effective and promising for problems of solar-terrestrial physics.

The NN architecture we have proposed in this paper, based on time series of matrix MH observations, exceeds in efficiency the approach described in [Belov et al., 2022; Getmanov et al., 2022b] and based on the formation of scalar time series of function values (3) from matrix MH observations.

## CONCLUSION

1. The GMS recognition method we have developed in the paper by analyzing and processing time series of matrix observations with the muon hodoscope URAGAN, using deep learning NN, has proved to be efficient.

2. As a result of the research and computational experiments, we have selected the NN architecture ResNet34 and the dimension of input matrix package  $\Delta n = 60$ , which are most suitable for the problem considered.

3. Using experimental studies of the proposed GMS recognition algorithms on the control dataset, we have obtained probability estimates characterizing the quality of GMS recognition.

3.1. The results of calculations of the GMS recognition probabilities in the control period have allowed us to conclude that for the threshold  $Y_{D0} = -45$  nT, when the restriction condition for the probability of false recognition  $\alpha = 0.02$  is met, the probability of correct recognition  $\beta = 0.875$ .

3.2. Digital processing of MH observations for the six-month control period has enabled us to estimate the probabilities of correct  $\beta = 0.8212$  and false  $\alpha = 0.0047$  GMS recognitions.

3.3. Analysis of GMS recognition with quality metrics  $G0$ ,  $G1$  has allowed us to establish that the MH observations at hand are in balance and to assign a suitable recognition threshold  $Y_{D0}^{\circ} = -35$  nT.

4. The experimental study has revealed that the proposed approach to the construction of DLNN, which is based on the use of time series consisting of MH observation matrices, is more effective than the approach described in [Belov et al., 2022; Getmanov et al., 2022a], which was based on the formation of scalar time series of average hourly MH observations from matrix MH observations.

5. The developed recognition method has shown promise and can be applied in many scientific and technical applications, for example, in the case of possible sudden absence (omission) of WDCG *Dst* indices, GMS recognition can be carried out using pre-built *Dst* index

models operating only with MH observations, as well as, if necessary, short-term forecasting of GMS, which can be implemented by extrapolating MH observations.

The work was supported by a project part of the Government Assignment from the Geophysical Center RAS and Schmidt Institute of Physics of the Earth RAS, approved by the Ministry of Science and Higher Education of the Russian Federation.

We are grateful to the executive team of The Unique Scientific Facility «Experimental complex NEVOD» MEPhI for providing observational data from the muon hodoscope URAGAN for calculations.

## REFERENCES

- Astapov I.I., Barbashina N.S., Borog V.V., Dmitrieva A.N., Shulzhenko I.A., Shutenko V.V., et al. *Muon Diagnostics of Earth's Magnetosphere and Atmosphere*. Moscow, MEPhI, 2014. 132 p. (In Russian).
- Ba J.L., Kingma D.P. Adam: A method for stochastic optimization. 3rd International Conference on Learning Representations, ICLR 2015 — Conference Track Proceedings. 2015, pp. 1–15.
- Barkhatov N.A. *Artificial Neural Networks in Solar-Terrestrial Physics*. Nizhny Novgorod, Povolzh'e, 2010. 707 p. (In Russian).
- Belov A.V., Gvishiani A.D., Getmanov V.G., Kovylyayeva A.A., Solovyev A.A., Chinkin V.E., et al. Identification of geomagnetic storms based on neural model estimates of *Dst* indices. *J. Computer and Systems Sciences International*. 2022, no. 1, pp. 56–66. (In Russian).
- Berngardt O.N. The first comparative analysis of meteor echo and sporadic scattering identified by a self-learning neural network in EKB and MAGW ISTEP SB RAS radar data *Solar-Terr. Phys.* 2022, vol. 8, iss. 4, pp. 63–72.
- Chen X., Yu R., Ullah S., Wu D., Zhiqiang Li Zh., Li Q., et al. A novel loss function of deep learning in wind speed forecasting. *Energy*. 2022, vol. 238, p. 121808.
- Chinkin V.E., Astapov I.I., Gvishiani A.D., Getmanov V.G., Dmitrieva A.N., Dobrovolsky M.N., et al. Method for the identification of heliospheric anomalies based on the functions of the characteristic deviations for the observation matrices of the muon hodoscope. *Physics of Atomic Nuclei*. 2019, vol. 82, no. 6, pp. 924–928.
- Dolenko S.A., Orlov Yu.V., Persianinov I.G., Shugai Ju.S. Neural network algorithm for events forecasting and its application to space physics data. *Lecture Notes in Computer Science*. 2005, vol. 3697, pp. 527–532.
- Getmanov V.G., Chinkin V.E., Gvishiani A.D., Dobrovolsky M.N., Sidorov R.G., Soloviev A.A., et al. Application of indicator matrices for the recognition of local anisotropies of muon fluxes in time series of matrix observations of the URAGAN hodoscope. *Pattern Recognition and Image Analysis: Adv. in Mathematical Theory and Applications*. 2022a, vol. 32, no. 3, pp. 717–728.
- Getmanov V.G., Chinkin V.E., Gvishiani A.D., Sidorov R.V., Gvishiani A.D., Dobrovolskii M.N., Solov'ev A.A., et al. Geomagnetic storm prediction based on the neural network digital processing of joint observations of the URAGAN muon hodoscope and neutron monitor stations. *Geomagnetism and Aeronomy*. 2022b, vol. 62, iss. 4, pp. 388–398.
- Gruet M.A., Chandorkar M., Sicard A., Camporeale E. Multiple-hour-ahead forecast of the *Dst*-index using a combination of long short-term memory neural network and Gaussian process. *Space Weather*. 2018, vol. 16, iss. 11, pp. 1882–1896. DOI: [10.1029/2018SW001898](https://doi.org/10.1029/2018SW001898).

- Efitorov A.O., Myagkova I.N., Shirokii V.P., Dolenko S.A. The prediction of the *Dst*-index based on machine learning methods. *Cosmic Res.* 2018, vol. 56, iss. 6, pp. 434–441.
- Lundstredt H. Geomagnetic storm predictions from solar wind data with the use of dynamic neural networks. *J. Geophys. Res.* 1997, vol. 102, no. A7, pp.14,255–14,268.
- Murzin V.S. *Astrophysics of Cosmic Rays*. Moscow, 2007. 488 p.
- Myagkova I.N., Shirokii V.R., Vladimirov R.D., Barinov O.G., Dolenko S.A. Prediction of the *Dst*-index using adaptive methods. *Russian Meteorology and Hydrology*. Al-lerton Press Inc. 2021, vol. 46, no. 3, pp. 157–162.
- Pallochia G., Amota E., Consolini G., Marcucci M.F., Bertello I. Geomagnetism *Dst*-index forecast based on IMF data only. *Ann. Geophys.* 2006, vol. 24, pp. 989–999.
- Stepanova M.V., Perez P. Autoprediction of *Dst*-index using neural network techniques and relationship to the auroral geomagnetism indices. *Geofisica International*. 2000, vol. 39, no. 1, pp. 143–146.
- Suigiura M. Hourly values of equatorial *Dst* for the IGY. *Ann. Int. Geophys. Year*. Pergamon Press, Oxford. 1964, vol. 35, pp. 9–45.
- Yashin I.I., Astapov I.I., Barbashina N.S., Bogod V.V., Chernov D.V., Dmitieva A.N., et al. Real-time data of muon hodoscope URAGAN. *Adv. Space Res.* 2015, vol. 56, iss. 12, pp. 2693–2705.
- URL: <https://wdc.kugi.kyoto-u.ac.jp> (accessed December 23, 2023).
- URL: <http://www.nevod.mephi.ru/> (accessed March 13, 2024).
- URL: <https://it.mephi.ru/hpc/performance> (accessed December 23, 2023).
- URL: <https://arxiv.org/abs/1905.11946/> (accessed December 23, 2023).
- URL: <https://arxiv.org/abs/1409.1556v6> (accessed December 23, 2023).
- URL: <https://arxiv.org/abs/1608.06993v5> (accessed December 23, 2023).
- URL: <https://arxiv.org/abs/1512.00567v3> (accessed March 13, 2024).
- URL: <https://arxiv.org/pdf/2107.07699.pdf> (accessed December 23, 2023).
- URL: <https://arxiv.org/abs/1512.03385> (accessed December 23, 2023).
- URL: <https://arxiv.org/pdf/1412.6980.pdf> (accessed December 23, 2023).
- URL: <https://pytorch.org/docs/stable/generated/torch.optim.Adam.html> (accessed December 23, 2023).
- URL: <https://learndatasci.com/glossary/binary-classification/> (accessed October 23, 2023).
- URL: <https://www.learndatasci.com/glossary/binary-classification/> (accessed March 13, 2024).
- URL: <https://helenkapatsa.ru/blogpost/otsienka-f1> (accessed March 13, 2024).
- URL: <https://www.izmiran.ru/ionosphere/weather/storm/> (accessed March 13, 2024).
- Original Russian version: Getmanov V.G., Gvishiani A.D., Soloviev A.A., Zajtsev K.S., Dunaev M.E., Ehlaikov E.V., published in *Solnechno-zemnaya fizika*. 2024. Vol. 10. Iss. 1. P. 83–91. DOI: [10.12737/szf-101202411](https://doi.org/10.12737/szf-101202411). © 2023 INFRA-M Academic Publishing House (Nauchno-Izdatelskii Tsentr INFRA-M)
- How to cite this article*
- Getmanov V.G., Gvishiani A.D., Soloviev A.A., Zajtsev K.S., Dunaev M.E., Ehlaikov E.V. Recognition of geomagnetic storms from time series of matrix observations with the muon hodoscope URAGAN using neural networks of deep learning. *Solar-Terrestrial Physics*. 2024. Vol. 10. Iss. 1. P. 76–83. DOI: [10.12737/stp-101202411](https://doi.org/10.12737/stp-101202411).